

TiO₂/TiN interface enables integration of Ni₅P₄ electro-catalyst with a III-V tandem photoabsorber for stable unassisted solar-driven water splitting

Shinjae Hwang^{a,‡}, Hengfei Gu^{a,‡}, James L. Young^b, Myles A. Steiner^b, Anders B. Laursen^a, Ryan A. Crichton^a, Yao-Wen Yeh^c, Philip E. Batson^c, Leonard C. Feldman^{c, d}, Mengjun Li^a, Keenan Wyatt^b, Ahmad Safari^d, Todd G. Deutsch^b, Eric Garfunkel^{a, *} and G. Charles Dismukes^{a, e*}

^aDepartment of Chemistry and Chemical Biology, Rutgers, The State University of New Jersey, Piscataway, New Jersey 08854, United States

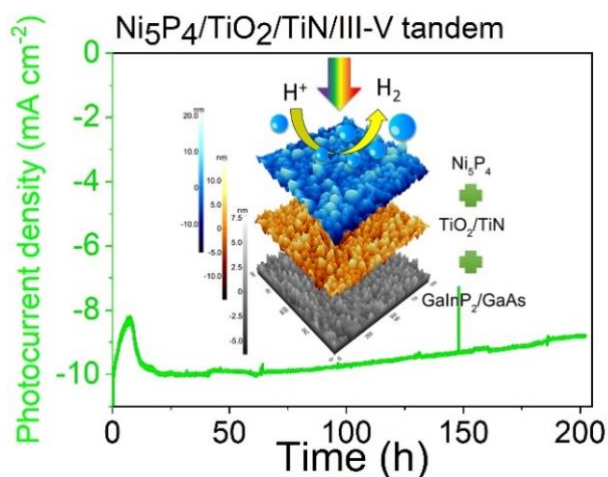
^bNational Renewable Energy Laboratory, 15013 Denver West Parkway, Golden, Colorado 80401, United States

^cDepartment of Physics and Astronomy, Rutgers, The State University of New Jersey, Piscataway, New Jersey 08854, United States

^dDepartment of Materials Science & Engineering, Rutgers, The State University of New Jersey, Piscataway, New Jersey 08854, United States

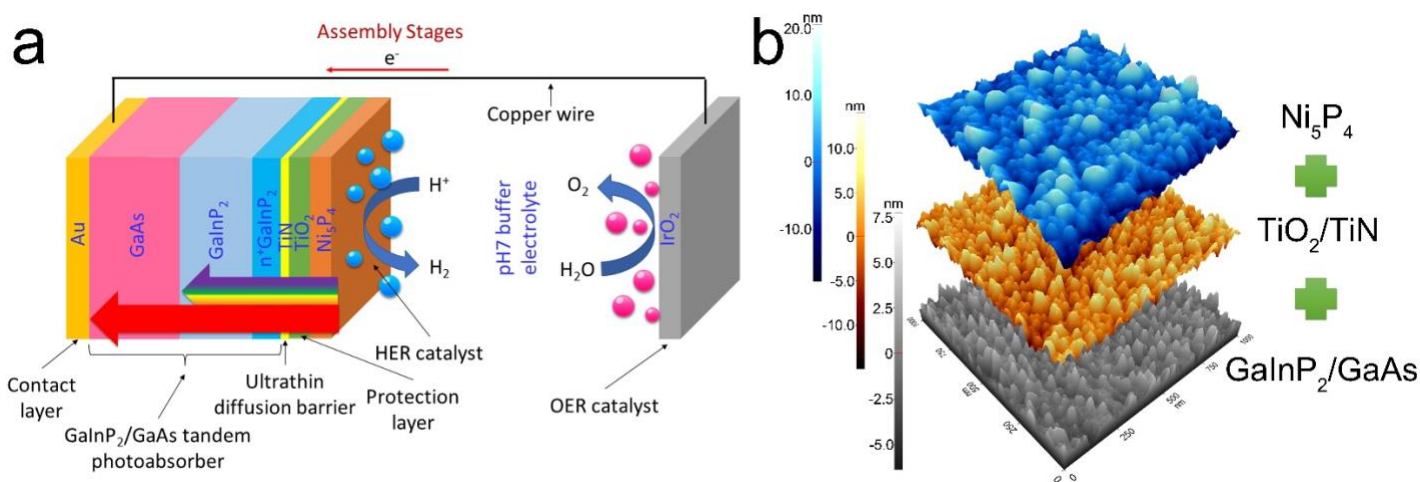
^eWaksman Institute, Rutgers, The State University of New Jersey, Piscataway, New Jersey 08854, United States

ABSTRACT: H₂ production by direct photoelectrochemical (PEC) water splitting has remained unachievable commercially mainly due to rapid failure at the interface between the photoabsorber(s) and catalyst(s). PEC devices made from multijunction III-V semiconductors with platinum group metal (PGM) catalysts have yielded impressive initial solar-to-H₂ (STH) efficiency > 19%, that rapidly corrodes in aqueous electrolytes. Here, TiO₂/TiN layers were fused to create a bifunctional interface between a GaInP₂/GaAs III-V tandem photoabsorber and a polycrystalline Ni₅P₄ HER catalyst. The TiO₂ serves as a conducting corrosion barrier, while a thin layer of much denser TiN (1 nm) blocks inter-layer diffusion during fabrication. This strategy allows elevated temperatures needed to crystallize the Ni₅P₄ nanoparticles and fuse to the TiO₂/TiN junction to achieve minimal optical loss and without damaging the sensitive photoabsorber. The resulting photocathode exhibits an initial STH efficiency of 11.4% - 13.2% in sodium phosphate electrolyte at neutral pH7. It operated continuously for over 200 h without failure above 10% STH efficiency, exceeding all previous benchmarks. The earth-abundant Ni₅P₄ catalyst replaces costly PGM catalysts at comparable HER activity in neutral, acidic or basic pH electrolytes.



Future sustainable energy usage will rely upon on the efficient, low-cost, long-term conversion of solar energy into a pollution-free, high-energy density fuels like hydrogen.¹⁻³ Photoelectrochemical (PEC) water splitting is considered a promising pathway towards solar-driven hydrogen production by using an integrated device comprised of solar absorbers and catalysts for sunlight harvesting and electrolysis, respectively.⁴⁻⁷ An efficient photoabsorber material is p-type GaInP₂, which has a bandgap of ~ 1.8 eV that is nearly optimal for a wide-

bandgap junction in a tandem solar cell.^{6, 8-11} Monolithic tandem semiconductors coupling a GaInP₂ top junction with a lower-bandgap bottom junction such as GaAs or lattice-mismatched GaInAs have achieved extremely high power conversion efficiencies (PCEs). This has motivated efforts to make PEC cells from them.⁶ Among the laboratory-developed PEC devices, the III-V semiconductor photoelectrodes have yielded the highest solar-to-hydrogen (STH) efficiencies under simulated one-sun illumination of ~ 19% and ~ 16% using a Rh/TiO₂/Ga_{0.41}In_{0.59}P/Ga_{0.89}In_{0.11}As tandem photocathode and an inverted metamorphic PtRu/Ga_{0.51}In_{0.49}P/Ga_{0.89}In_{0.11}As tandem photocathode, respectively.^{6, 12, 13} However, these devices lost ~ 31% and ~ 15% activity in the first 0.5 and 1.4 h, respectively, due to photocorrosion. Practical solar hydrogen production using III-V materials has remained unrealized due to their photocorrosion and inherent thermodynamic instability in aqueous electrolytes over a wide range of pH, especially acidic and alkaline electrolytes.^{7, 14-16} Other emerging thin-film photoabsorbers are being developed that face similar challenges, such as hybrid organic-inorganic perovskites, based on monolithic photoelectrodes for unassisted PEC water splitting.¹⁷⁻¹⁹



Scheme 1. Schematic illustration of III-V tandem photocathode for HER applications (a) and surface topological images of the photocathode and its modification layers without and with a catalyst layer (b). The photocathode is made up of an integrated catalyst:tandem photoabsorber combination of Ni₅P₄/TiO₂/TiN(catalyst/protection layer/diffusion barrier) plus GaInP₂/GaAs. It performs water splitting under solar illumination in combination with an anode with OER catalysts (IrO₂ particles).

One strategy to slow photocorrosion of GaInP₂ under HER conditions is to functionalize its surface. Electronic and chemical passivation has been achieved by applying a tightly bonded layer of ultrathin AlInP and subsequently oxidizing it.²⁰ This slowed the PEC degradation in acid when used with noble metal catalysts, but resulted in short-lived durability. An analogous strategy is to add a conductive, optically transparent protection barrier.¹⁵ Several transition metal sulfides, oxides and nitrides have been investigated as potential protection layers. A MoS₂ thin film was integrated onto a p-GaInP₂ single junction photocathode by sulfidation of a Mo thin film that played a bifunctional role as protection layer and HER catalyst.²¹ This process stabilized the photocathode for 60 h in acid without loss of activity, but degraded thereafter. MoS₂ has been coated on p-GaInP₂ also by photoelectro-deposition, achieving a marginally better combination of activity and durability (50 h in acid with ~ 14% loss of the photocurrent density).¹⁰ Applying a MoS₂ thin film on III-V tandem enabled a STH efficiency of 6.1% and a durability of 120 h with ~ 23% loss of efficiency in acid under simulated 2.6-sun illumination.²² In addition to MoS₂, a TiO₂ thin film was used to protect GaInP₂/GaAs photoanode.²³ The resulting photoanode exhibited a STH efficiency of 10% in a 0.5 M potassium borate solution (KBi, pH 9.3) and performed

unassisted water splitting for 100 h, the longest PEC durability so far. Similarly, a GaN coating on a GaInP₂/GaAs/Ge triple-junction cell has been shown to protect the absorber from degradation.²⁴ When used with Pt nanoparticles as catalyst, a peak STH efficiency of 12.6% and stability of 70 h with ~ 29% loss of efficiency in acid was achieved.

GaInP₂ exhibits poor intrinsic electrocatalytic activity for reduction of protons or water and must therefore be coupled to an additional catalyst layer.^{10, 25} A graded MoS₂/MoO_yS_z/MoO_x coating as catalyst with TiO₂ has been found to slow photocorrosion of p-GaInP₂ allowing operation for 20 h in acid. However, performance was likely compromised by significant inter-layer diffusion of elements at the TiO₂/GaInP₂ interface (~70 nm inter-layer diffusion region).²⁶ Other problems such as pin holes in the protection layer have limited the durability of atomic layer deposited TiO₂ used to protect III-V triple-junction photocathodes. For example, Pt/TiO₂/Ti/GaInP/GaAs/Ge photocathode exhibited a limited durability in acid (a loss of STH efficiency of ~ 52% within 72 h).²⁷ The foregoing reports all identify failure at the electrolyte/catalyst/photoabsorber interface as the weakest component in PEC devices. Inter-layer diffusion (loss of interface) and corrosion are the root cause of these failures.

Previously, we reported using TiN as a diffusion barrier to allow use of elevated temperature for synthesis of crystalline Ni₅P₄ particles at the interface of p-GaInP₂ single junction photocathode. This procedure enabled operation for 120 h in acid at 0.25 V vs reversible hydrogen electrode (RHE) without any losses using a three-electrode measurement configuration. This strategy did not work using TiO₂ alone.¹⁷ TiN exhibits exceptional chemical and physical properties, including high conductivity, high density and hardness, and good corrosion resistance.²⁸ Herein, we use a bifunctional protection/diffusion barrier composed of crystalline TiO₂/TiN that permits device fabrication at even higher temperatures needed to synthesize crystalline Ni₅P₄ electro-catalyst for HER and functionally connect it to the III-V tandem photoabsorber via a conducting n⁺-GaInP₂ layer. To minimize optical losses and maintain a high saturated photocurrent density, we reduce the thickness of TiN to 1 nm. To retard photo-corrosion by the electrolyte, a pH7 solution of 0.5M sodium phosphate was used as the buffered electrolyte. The designed Ni₅P₄/TiO₂/TiN/III-V tandem photocathode is illustrated in **Scheme 1** and the fabrication metrics are described below. To demonstrate unassisted solar water splitting and assess the STH efficiency and durability for solar hydrogen production, we use a two-electrode measurement configuration.²⁹

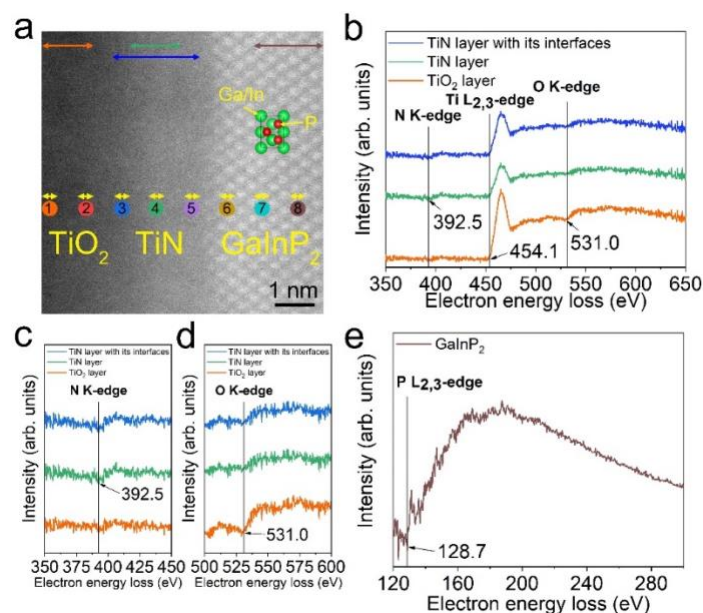


Figure 1. Deposition of 1 nm thick TiN between TiO₂ and GaInP₂. **a**, HAADF cross-sectional image of the TiO₂/TiN/GaInP₂ interface of the Ni₅P₄/TiO₂/TiN/III-V tandem photocathode, revealing co-alignment of the [110] axis of FCC-structured GaInP₂. EELS mapping was carried out on this cross-sectional region. Integration of the EELS spectra was performed on a rectangular region equal in size to the double headed arrows. **b**, The integrated EELS spectra of the layers of TiO₂, TiN and TiN with its TiO₂ and GaInP₂ interfacial regions (the measured layer thicknesses are indicated by the orange, green and blue arrows shown in **a**, respectively). **c** and **d**, Zoomed-in EELS spectra in **b**. **e**, The integrated EELS spectrum of the GaInP₂ layer (the measured layer thickness is indicated by the brown arrow in **a**).

The chosen photoabsorber is a lattice-matched, upright-grown GaInP₂/GaAs tandem, fabricated by epitaxial growth using a metal organic vapor-phase epitaxy (MOVPE) reactor (see **Supplementary Information** for this and following procedures).^{8,30} Prior to integration of the layers, the surface of GaInP₂ was first etched using the NH₄F/HF (denoted buffered oxide etchant or BOE). This treatment removed all surface oxides including Ga₂O₃, In₂O₃, and PO_x, while not dissolving the GaInP₂ photoabsorber surface.¹¹ The TiN diffusion barrier and TiO₂ protection layers were subsequently deposited on to the III-V tandem samples by pulsed laser deposition (PLD), starting from the respective solids. For comparison, we deposited the TiO₂ protection layer alone onto the III-V tandem samples using the same method. The resulting TiO₂/III-V tandem and TiO₂/TiN/III-V tandem samples were annealed at 375 °C in vacuum (~1×10⁻⁶ torr). The Ni₅P₄ compound was synthesized *in situ* on the surface-modified III-V tandem photoabsorbers, first by thermal evaporation of a 2 nm Ni layer, followed by high-temperature phosphidation of the pre-deposited Ni layer with red phosphorus (P) at 375 °C in an air-evacuated quartz ampoule. This step was followed by appropriate furnace cooling and air quenching.¹¹ Using this protocol and by optimizing the phosphidation conditions especially the P pressure at 375 °C, we are able to synthesize phase-pure Ni₅P₄ crystallites with a thickness of ~10 nm that form interconnected islands. The sample surface roughness (R_q) was measured by atomic force microscopy (AFM) (**Supplementary Figure S1**). R_q values equal to 3 or 4 nm after adding the aforementioned layers. The composition of the surface layer was analyzed by X-ray photoelectron spectroscopy (XPS) (see details in **Supplementary Figure S2 and Table S1**).

Previously, we measured the transmission, reflection and absorptance between wavelengths 380 to 800 nm of a 4 nm thick film of PLD-deposited TiN.³¹ Here, we sought to reduce the thickness further to improve the optical transmission. The optical losses from the Ni₅P₄/TiO₂/TiN layers arise mainly from the absorption of TiO₂ at shorter wavelengths and by absorption from Ni₅P₄ and TiN at longer wavelengths (**Supplementary Figure S3**).

Figure 1a gives a cross-sectional image of the TiO₂/TiN/GaInP₂ interface after Ni₅P₄ synthesis of the final PEC device. This image was observed by high-resolution transmission electron microscopy (HRTEM) along the [110] direction of face-centered cubic (FCC)-structured GaInP₂ by high angle annular dark field (HAADF) technique. As the ternary Ga-In-P system forms solid solutions, GaInP₂ has the same zincblende-type FCC structure as GaP (F $\bar{4}3m$ space group, JCPDS-88-2491) and InP (F $\bar{4}3m$ space group, JCPDS-73-1983), and its lattice parameter falls between that of GaP and InP.³² The FCC structure is confirmed by the atomic pattern in **Figure 1a** and by fast Fourier transformation (FFT) analysis (**Supplementary Figure S4d**). The PLD procedure creates a uniform TiN layer of ~ 1 nm thickness and relatively brighter contrast vs TiO₂. The brighter contrast from this layer arises from the higher angle scattering of electrons and reveals the presence of the high density TiN material. FFT analysis reveals that both TiN and TiO₂ layers are amorphous (**Supplementary Figure S4b and c**). Our recent work discovered that annealing of the physical vapor deposited TiO₂/TiN on n⁺-Si at 300 °C results in formation of crystalline anatase phase of TiO₂.¹⁷ It may be feasible to use air annealing of TiO₂/TiN/GaInP₂ to form a crystalline TiO₂ layer for future tests of further durability improvement.

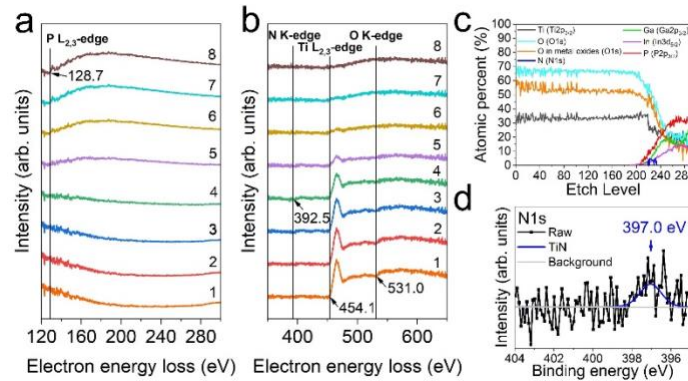


Figure 2. The influence of adding a 1 nm TiN layer on the inter-layer diffusion of elements within the TiO₂/GaInP₂ interface during high-temperature synthesis. **a** and **b**, The integrated EELS spectra measured at Positions #1-8 in **Figure 1a**. **c**, XPS depth profiles of elemental composition (atomic %) of 30nmTiO₂/1nmTiN/III-V tandem. **d**, the N1s spectrum of 1 nm TiN at the TiO₂/GaInP₂ interface obtained during the XPS depth profiling. For each etch level during depth profiling, Ar⁺ sputtering at an energy of 500 eV was carried out for 60 s on the sample surface 2 mm in diameter.

Electron energy loss spectroscopy (EELS) and XPS, together with TEM imaging were used to determine the chemical states and bonding partners around the excited atoms as a function of depth. In the core EELS spectra, the TiO₂ layer is identified by the Ti L_{2,3}-edge at 454.1 eV and O K-edge at 531.0 eV, while the TiN layer is identified by Ti L_{2,3}-edge at almost the same energy and N K-edge at 392.5 eV (**Figure 1b-d**).³³ Also, a small O K-edge peak is found within the TiN layer. This is likely due to formation of TiON, which is confirmed by the XPS results (**Supplementary Figure S2a-c**). The oxygen may arise from the hydroxides on the BOE-etched GaInP₂ surface prior to the TiN deposition.¹⁷ The P L_{2,3}-edge is identified within the GaInP₂ layer (**Figure 1e**).

EELS analysis along the depth direction was performed to examine inter-layer diffusion (EELS Spectra #1-8 in **Figure 2a** and **b** corresponding to Position #1-8 in **Figure 1a**). The P L_{2,3}-edge peak is not seen within the TiN and TiO₂ layers (Spectra #1-5 in **Figure 2a**), indicating the successful blocking of P diffusion into the TiO₂ layer by the 1 nm thick TiN. The O K-edge peak cannot be observed within the GaInP₂ absorber layers, indicating prevention of diffusion of O from outer layers into the GaInP₂ (Spectra #6-8 in **Figure 2b**). However, the Ti L_{2,3}-edge peak but not the N K-edge peak was found within the first three atomic layers of GaInP₂, indicating a low degree of diffusion of Ti into the GaInP₂. Both our recent work and the literature work reveal that Ti from TiN can diffuse into Si during annealing above 300 °C.^{17, 34} XPS depth profiling (**Figure 2c**) gave results consistent with the EELS profiling, demonstrating both the thickness and localization of the TiN layer. The sample, 30nmTiO₂/1nmTiN/III-V tandem, was pre-annealed at 375 °C in a high vacuum for 30 min. The surface has a Ti:O composition slightly under the stoichiometry of TiO₂. Between the TiO₂ and GaInP₂ layers, a small N1s peak was detected at binding energy of 397.0 eV that results from TiN (**Figure 2d**). The corresponding N profile is plotted in blue color (**Figure 2c**). It demonstrates that N remained localized at the interface and that inter-layer diffusion between TiO₂ and GaInP₂ did not occur during the elevated temperature annealing. The ultrathin TiN layer successfully stopped the atoms of Ga, In and P from penetrating into the TiO₂ layer.

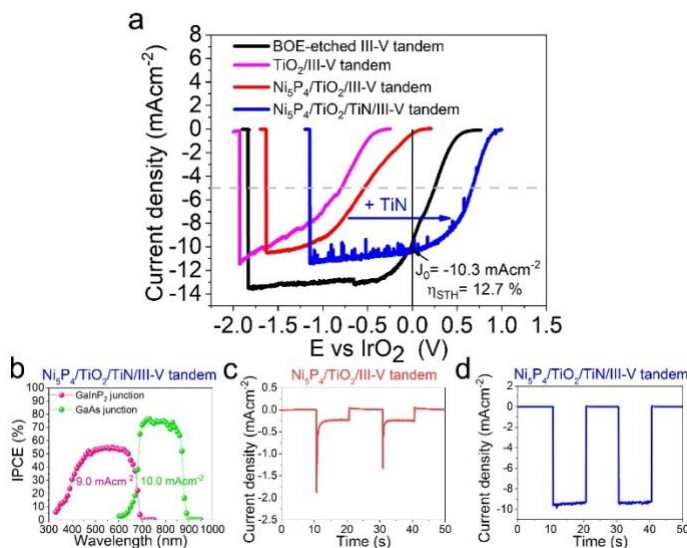


Figure 3. PEC analysis of the catalyst/protection layer-coated or catalyst/protection and diffusion barrier bilayers-coated GaInP₂/GaAs III-V tandem photocathodes in pH7 sodium phosphate buffer solution under one-sun illumination. **a**, LSV curves of Ni₅P₄/TiO₂/III-V tandem and Ni₅P₄/TiO₂/TiN/III-V tandem photocathodes compared to the bare III-V tandem and TiO₂/III-V tandem interfaces, measured in a two-electrode configuration. **b**, IPCE of the Ni₅P₄/TiO₂/TiN/III-V tandem photocathode measured at zero bias in a two-electrode configuration. **c** and **d**, the photocurrent responses of Ni₅P₄/TiO₂/III-V tandem and Ni₅P₄/TiO₂/TiN/III-V tandem obtained using alternating light on/off conditions at zero bias. Note the different current scales.

The PEC activity was evaluated in a two-electrode configuration, in which an anode made from IrO₂-coated carbon paper was kept in neutral electrolyte (0.5 M sodium phosphate solutions, pH7). The resulting Faradaic efficiency for the oxygen evolution reaction was > 95% (**Supplementary Table S2**). Illumination was done under simulated AM 1.5G solar illumination. The representative current density-voltage (*J*-*V*) curves are shown in **Figure 3a**. There was no measurable HER activity for any of the tested photocathodes under dark conditions in the bias voltage window. The BOE-etched III-V tandem showed a saturated photocurrent density, *J*_{sat}, of -13.4

mAcm^{-2} , which is larger than that obtained in the photovoltaic J-V curve measured in air (-9 mAcm^{-2} , **Supplementary Figure S5**). This gain was shown to be due to the removal of surface oxides and the reduced reflection at the photoabsorber/electrolyte interface compared to the air interface.³⁰ The $\text{Ni}_5\text{P}_4/\text{TiO}_2/\text{TiN}/\text{III-V}$ tandem photocathode exhibited a J_{sat} of -11.3 mAcm^{-2} and a photocurrent density at zero bias, J_0 , of -10.3 mAcm^{-2} , corresponding to a STH efficiency of 12.7%. The measured J_{sat} is lower than that of bare III-V due to light absorption by the $\text{Ni}_5\text{P}_4/\text{TiO}_2/\text{TiN}$ layers. The high J_0 confirms the good HER catalytic activity of the Ni_5P_4 catalyst in neutral electrolyte. Measurements of replicates showed a range of J_0 values from -9.3 to -10.7 mAcm^{-2} , corresponding to a STH efficiency between 11.4% and 13.2%. An almost identical J_{sat} was achieved using the photocathodes without the 1 nm thick TiN diffusion barrier ($\text{TiO}_2/\text{III-V}$ tandem and $\text{Ni}_5\text{P}_4/\text{TiO}_2/\text{III-V}$ tandem). This indicates that the ultrathin TiN layer is highly transparent and does not appreciably compromise the photocurrent density. By contrast, the unprotected electrode exhibited a significant negative shift of $\sim -1.04 \text{ V}$ to achieve a photocurrent density of -5 mAcm^{-2} for the $\text{TiO}_2/\text{III-V}$ tandem photocathode referenced to bare III-V tandem. Adding Ni_5P_4 imparts some activity to the $\text{Ni}_5\text{P}_4/\text{TiO}_2/\text{III-V}$ tandem, indicated by the anodic shift of its J-V curve compared to that of $\text{TiO}_2/\text{III-V}$ tandem, but the improvement is significantly smaller below 30% compared to the case with the additional TiN layer present. The squareness of the J-V curves (Fill Factor) of the $\text{Ni}_5\text{P}_4/\text{TiO}_2/\text{TiN}/\text{III-V}$ tandem and the bare III-V tandem is comparable. However, the J-V curves of the tandem photocathodes lacking the TiN diffusion barrier have appreciably smaller squareness. As the 1 nm thick TiN succeeded in blocking the inter-diffusion between TiO_2 and GaInP_2 , as revealed by the EELS and XPS results above, the loss of squareness without the TiN layer can be attributed to the enhanced inter-diffusion at the $\text{TiO}_2/\text{GaInP}_2$ interface during the elevated temperature annealing.²⁶ Such inter-diffusion likely results in the formation of Ga_2O_3 , In_2O_3 , and PO_x , thereby increasing the series resistance of the photoelectrodes and thus lowering the J-V curve squareness.³⁵ Also, consumption of the conductive n^+ - GaInP_2 layer due to inter-layer diffusion could retard the separation of light-induced carriers and reduce the photovoltage.

Figure 3b shows the incident photon-to-current efficiency (IPCE) of the $\text{Ni}_5\text{P}_4/\text{TiO}_2/\text{TiN}/\text{III-V}$ photocathode measured in the same neutral electrolyte under zero-bias conditions as a function of wavelengths in the visible light range. The top GaInP_2 junction absorbs and converts the photons that have energies $\geq 1.8 \text{ eV}$ to photocurrent with IPCE in the range of 0 - 54% from 330 - 750 nm. Photons with lower energies and long wavelengths were transmitted through the top junction and are absorbed by the bottom GaAs junction, resulting in additional photocurrent with IPCE in the range of 0 - 75% from 600 - 950 nm. The photocurrent densities that are generated by the individual top and bottom junctions are calculated to be 9.0 and 10.0 mAcm^{-2} respectively, by integrating the IPCE over a reference solar spectrum standard (AM 1.5 G, ASTM G173-3). The device photocurrent density is limited by the top junction, which is slightly lower than the absolute J_0 values obtained in the LSV curve. The IPCE confirms the high photon-conversion efficiency of the $\text{Ni}_5\text{P}_4/\text{TiO}_2/\text{TiN}/\text{III-V}$ tandem photocathode across the visible spectrum and that the thickness of the GaInP_2 top junction should be increased slightly for a better current match in the tandem.

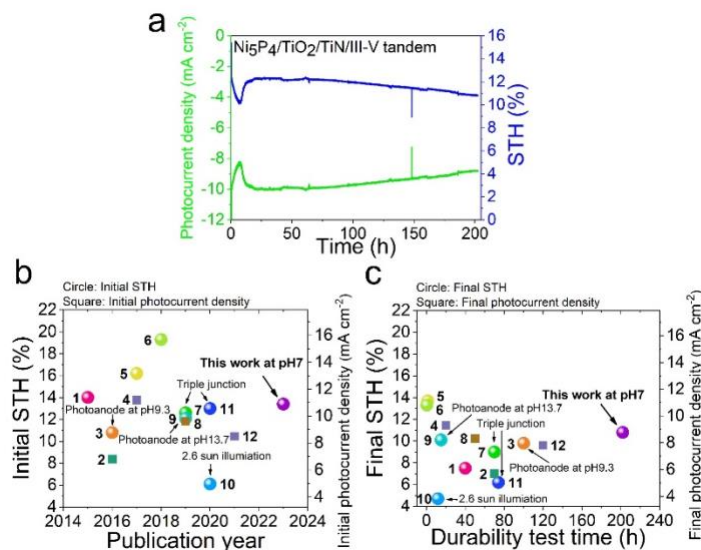


Figure 4. Durability comparison of the catalyst/protection and diffusion barrier bilayers-coated GaInP₂/GaAs III-V photocathode with other surface modified III-V photoelectrodes reported in the literature (see Supplementary Table S3 and 4). **a**, CA curve and the corresponding STH efficiency as a function of time of the Ni₅P₄/TiO₂/TiN/III-V tandem photocathode measured in pH7 sodium phosphate buffer solution under one-sun illumination in a two-electrode configuration. **b**, Initial photocurrent densities of GaInP₂ single junction photocathode measured at or near 0 V vs RHE and initial STH efficiencies of III-V multijunction photoelectrodes that are calculated from the unbiased photocurrent density measured in a two-electrode configuration. The squares and circles represent the single junction photoelectrodes and the tandem or triple junction photoelectrodes, respectively. Most of the multiple junction photoelectrodes are tandem, while the triple junction is labeled. Most of the photoelectrodes were evaluated under one-sun illumination, while the more concentrated illumination is labeled. Most of the photoelectrodes were examined in acid at pH 0, while the other pH conditions are labeled. **c**, The corresponding final photocurrent densities and final STH efficiencies of the compared photoelectrodes after the durability tests. The compared photoelectrodes are as follows: 1: Rh/Surface oxidized AlInP/III-V tandem photocathode;²⁰ 2: MoS₂+Mo/p-GaInP₂ photocathode;²¹ 3: Ni/amorphous TiO₂/III-V tandem photoanode;²³ 4: MoS_x/MoO_yS_z/MoO_x/crystalline TiO₂/p-GaInP₂ photocathode;²⁶ 5: PtRu/n-GaInP/n-AlInP/n-GaInP/III-V tandem photocathode;⁶ 6: RuO_x/GaAs/III-V tandem/AlInP/AlInPO_x/crystalline TiO₂/Rh photoelectrode;¹² 7: Pt/n-GaN/GaInP₂/GaAs/Ge triple junction photocathode;²⁴ 8: MoS_x/p-GaInP₂ photocathode;¹⁰ 9: Ni/AuBe/Au/GaAs/GaInP tandem photoanode,³⁶ 10: MoS₂/III-V tandem photocathode;²² 11: Pt/TiO₂/Ti/GaInP/GaAs/Ge triple photocathode²⁷ and 12: Ni₅P₄/TiN/n⁺p-GaInP₂ photocathode.¹¹

The photocurrent responses of the photocathodes with and without the ultrathin TiN diffusion barrier were measured by chronoamperometry (CA) under zero bias in a two-electrode configuration under alternating dark and light (one-sun illumination) conditions with a fixed time interval (**Figure 3c and d, respectively**). Significant photocurrent loss and transients in the response were observed for the photocathode without TiN, indicating charge recombination of light-induced carriers likely occurs within the photocathode under illumination. By contrast, a large photocurrent and stable response were observed for the photocathode with the 1 nm thick TiN interface. This indicates that no significant charge recombination is detectable between the Ni₅P₄/TiO₂/TiN/GaInP₂/GaAs interfaces nor the anode/contact interfaces at the start. The light-induced

photocurrent densities observed at zero bias for the two electrodes are consistent with the ones obtained from the J-V curves. These results demonstrate the effectiveness of the ultrathin TiN as a diffusion barrier during the high-temperature fabrication processes.

To evaluate the interfacial durability during PEC operation for hydrogen production, CA measurements were performed at zero bias under one-sun illumination for the Ni₅P₄/TiO₂/TiN/III-V tandem photocathode under the same two-electrode configuration for the LSV measurements (**Figure 4a**). At the beginning of the durability test, the cathodic photocurrent density was -10.7 mAcm⁻² and exhibited a rapid decay losing ~ 22% within the initial 7.5 h, then recovering nearly completely to a steady value of -10 mAcm⁻² within the next ~12 h. The initial 25 h durability is reproduced and shown in **Supplementary Figure S6**. The transient loss and recovery process was identified as due to migration of epoxy from internal masking unto the catalyst surface (see **Supplementary Figure S7-13**). After that, stable performance was observed until operation for ~ 60 h. After 60 h, a slow decrease in the photocurrent density occurs. Testing was stopped when STH efficiency was dropped to around 10%. The corresponding STH efficiency curve calculated based on the zero-biased photocurrent densities is also shown in **Figure 4**, where the photocurrent density had fallen to -8.8 mAcm⁻², corresponding to a STH efficiency of 10.8%. The total loss of photocurrent current density was ~ 18% over 202 h, which is the longest trial attempted among our triplicate tests at the same photocurrent loss (**Supplementary Figure S14**). The surface layers of Ni₅P₄/TiO₂ remained intact after the > 200 h durability test, and no out-diffusion of elements of Ga and In from the underneath photoabsorber (**Supplementary Figure S15**). The slow photocurrent decrease after 60 h is attributed to photoelectro-deposition of metallic copper and silver on the photoelectrode surface (**Supplementary Figure S13I and Figure S15e, g**).¹¹ These contaminants originate from fabrication of the anode (IrO₂-coated porous carbon paper that is composed of carbon fibers) using Cu wire and Ag paint. The same photocathode was also examined in 0.5M H₂SO₄ in a two-electrode configuration, showing a limited durability of ~ 2 h at a STH efficiency between 10.1% and 10.5% (**Supplementary Figure 16**).

The photoelectrodes and strategies reported in the literature are listed in **Supplementary Table S3 and 4**, together with our new data for Ni₅P₄/TiO₂/TiN/III-V tandem photocathode. The initial photocurrent densities measured in a three-electrode configuration and the initial STH efficiencies measured at zero bias in a two-electrode configuration for the single-junction and multiple-junction photoelectrodes, respectively, are plotted in **Figure 4b**. **Figure 4c** compares the final photocurrent densities and STH efficiencies measured after the durability tests for different times. Although not the highest STH efficiency, the photocathode reported herein and made using an Earth abundant HER catalyst exhibits stable STH efficiency ≥ 10% for the longest durability yet reported and without catastrophic failure of any of interfaces.

In summary, while surface passivation using a protection layer alone or a diffusion barrier alone can slow down the degradation of III-V-based photoelectrodes in corrosive electrolytes, we show here that the use of a bifunctional TiO₂/TiN interface gives synergistic improvement well beyond that of the individual materials. This is attributed to the different functions of these materials. The high density of TiN suppresses inter-layer diffusion between TiO₂ and GaInP₂ at elevated temperatures needed for synthesis of crystalline Ni₅P₄ catalyst and also contributes to protection of the unstable GaInP₂/GaAs tandem in the pH7 sodium phosphate buffer during PEC operation. Negligible photocurrent density was lost from the thin protective bilayers and Ni₅P₄ catalyst. This protection strategy enables the use of nickel phosphides as HER catalysts for the first time together with the high performance yet chemically fragile III-V tandem photoabsorbers. The combination of nickel phosphide catalyst and bilayer protection provides durability for at least 202 h of continuous hydrogen production above 10% STH efficiency. To the best of our knowledge, this is the longest durability of an integrated PEC device using

any catalyst for direct solar hydrogen production at this efficiency. This advance offer hope for continued improvements using these strategies and ultimately leading to commercial applications in the future.

AUTHOR INFORMATION

Corresponding authors

Eric Garfunkel - *Department of Chemistry and Chemical Biology, Rutgers, The State University of New Jersey, Piscataway, New Jersey 08854, United States, Email: egarf@chem.rutgers.edu*

G. Charles Dismukes - *Department of Chemistry and Chemical Biology, Rutgers, The State University of New Jersey, Piscataway, New Jersey 08854, United States; Waksman Institute, Rutgers, The State University of New Jersey, Piscataway, New Jersey 08854, United States, Email: dismukes@chem.rutgers.edu*

Authors

Shinjae Hwang - *Department of Chemistry and Chemical Biology, Rutgers, The State University of New Jersey, Piscataway, New Jersey 08854, United States*

Hengfei Gu - *Department of Chemistry and Chemical Biology, Rutgers, The State University of New Jersey, Piscataway, New Jersey 08854, United States*

James L. Young - *National Renewable Energy Laboratory, 15013 Denver West Parkway, Golden, Colorado 80401, United States*

Myles A. Steiner - *National Renewable Energy Laboratory, 15013 Denver West Parkway, Golden, Colorado 80401, United States*

Anders Laursen - *Department of Chemistry and Chemical Biology, Rutgers, The State University of New Jersey, Piscataway, New Jersey 08854, United States*

Ryan A. Crichton - *Department of Chemistry and Chemical Biology, Rutgers, The State University of New Jersey, Piscataway, New Jersey 08854, United States*

Yao-Wen Yeh - *Department of Physics and Astronomy, Rutgers, The State University of New Jersey, Piscataway, New Jersey 08854, United States*

Philip E. Batson - *Department of Physics and Astronomy, Rutgers, The State University of New Jersey, Piscataway, New Jersey 08854, United States*

Leonard C. Feldman - *Department of Physics and Astronomy, Rutgers, The State University of New Jersey, Piscataway, New Jersey 08854, United States; Department of Materials Science & Engineering, Rutgers, The State University of New Jersey, Piscataway, New Jersey 08854, United States*

Mengjun Li - *Department of Chemistry and Chemical Biology, Rutgers, The State University of New Jersey, Piscataway, New Jersey 08854, United States*

Keenan Wyatt - *National Renewable Energy Laboratory, 15013 Denver West Parkway, Golden, Colorado 80401, United States*

Ahmad Safari - *Department of Materials Science & Engineering, Rutgers, The State University of New Jersey, Piscataway, New Jersey 08854, United States*

Todd G. Deutsch - *National Renewable Energy Laboratory, 15013 Denver West Parkway, Golden, Colorado 80401, United States*

ACKNOWLEDGMENTS

This work was supported by the DOE-EERE (U.S. Department of Energy, Office of Energy Efficiency and Renewable Energy, Fuel Cell Technologies Office) Award# DE-EE0008083. The authors thank the Laboratory for Surface Modification (LSM) at Rutgers University for the XPS and TEM measurements, Prof. Deirdre O'Carroll's group for use of an integrating sphere for optical measurements and Prof. Martha Greenblatt's group for use of a furnace. The authors gratefully acknowledge research support from the HydroGEN Advanced Water Splitting Materials Consortium, established as part of the Energy Materials Network under the U.S. Department of Energy, Office of Energy Efficiency and Renewable Energy, Hydrogen and Fuel Cell Technologies Office, under Award Number DE-EE-0008084. This work was authored in part by the National Renewable Energy Laboratory, operated by Alliance for Sustainable Energy, LLC, for the U.S. Department of Energy under Contract Number DE-AC36-08GO28308. The views expressed in the article do not necessarily represent the views of the DOE or the U.S. Government. The U.S. Government retains and the publisher, by accepting the article for publication, acknowledges that the U.S. Government retains a nonexclusive, paid-up, irrevocable, worldwide license to publish or reproduce the published form of this work, or allow others to do so, for U.S. Government purposes.

AUTHOR CONTRIBUTIONS

Shinjae Hwang and Hengfei Gu: Conceptualization, Methodology, Formal analysis, Validation, Investigation, Data curation, Writing – original draft, Writing – review & editing. James L. Young and Myles A. Steiner: Methodology, Formal analysis, Validation, Investigation, Data curation, Writing – review & editing. Anders B. Laursen: Conceptualization, Methodology, Formal analysis, Investigation, Data curation, Writing – review & editing. Todd G. Deutsch: Methodology, Formal analysis, Writing – review & editing, Project administration. Eric Garfunkel and G. Charles Dismukes: Conceptualization, Methodology, Formal analysis, Writing – review & editing, Supervision, Project administration, Funding acquisition. The other authors: Formal analysis, Investigation, Data curation, Writing – review & editing.

COMPETING INTERESTS

The authors declare no competing financial interest.

ABBREVIATIONS

BOE: buffered oxide etchant
EELS: electron energy loss spectrum
HAADF: high angle annular dark field
HRTEM: high-resolution transmission electron microscopy
IPCE: incident photon-to-current efficiency
MOVPE: metal organic vapor-phase epitaxy
PCE: power conversion efficiency
PEC: photoelectrochemical
PGM: platinum group metal
PLD: pulsed laser deposition
STH: solar-to-hydrogen
XPS: X-ray photoelectron spectroscopy

REFERENCES

1. Turner, J. A., Sustainable hydrogen production. *Science* **2004**, *305* (5686), 972-974.
2. Nowotny, J.; Sorrell, C. C.; Sheppard, L. R.; Bak, T., Solar-hydrogen: Environmentally safe fuel for the future. *Int J Hydrogen Energ* **2005**, *30* (5), 521-544.
3. United States Department of Energy, Hydrogen and Fuel Cell Technologies Office, Hydrogen Storage.
4. Shaner, M. R.; Atwater, H. A.; Lewis, N. S.; McFarland, E. W., A comparative technoeconomic analysis of renewable hydrogen production using solar energy. *Energ Environ Sci* **2016**, *9* (7), 2354-2371.
5. Walter, M. G.; Warren, E. L.; McKone, J. R.; Boettcher, S. W.; Mi, Q. X.; Santori, E. A.; Lewis, N. S., Solar Water Splitting Cells. *Chem Rev* **2010**, *110* (11), 6446-6473.
6. Young, J. L.; Steiner, M. A.; Doscher, H.; France, R. M.; Turner, J. A.; Deutsch, T. G., Direct solar-to-hydrogen conversion via inverted metamorphic multi-junction semiconductor architectures. *Nat Energy* **2017**, *2* (4), 1-8.
7. Bullock, M.; More, K., Basic Energy Sciences Roundtable: Foundational Science for Carbon-Neutral Hydrogen Technologies (Report). *United States Department of Energy Office of Science and Office of Basic Energy Sciences* **2021**.
8. MacLeod, B. A.; Steirer, K. X.; Young, J. L.; Koldemir, U.; Sellinger, A.; Turner, J. A.; Deutsch, T. G.; Olson, D. C., Phosphonic Acid Modification of GaInP₂ Photocathodes Toward Unbiased Photoelectrochemical Water Splitting. *Acs Appl Mater Inter* **2015**, *7* (21), 11346-11350.
9. Geisz, J. F.; Steiner, M. A.; Garcia, I.; Kurtz, S. R.; Friedman, D. J., Enhanced external radiative efficiency for 20.8% efficient single-junction GaInP solar cells. *Applied Physics Letters* **2013**, *103* (4), 041118.
10. Lancaster, M.; Mow, R.; Liu, J.; Cheek, Q.; MacInnes, M. M.; Al-Jassim, M. M.; Deutsch, T. G.; Young, J. L.; Maldonado, S., Protection of GaInP₂ Photocathodes by Direct Photoelectrodeposition of MoS_x Thin Films. *Acs Appl Mater Inter* **2019**, *11* (28), 25115-25122.
11. Hwang, S.; Young, J. L.; Mow, R.; Laursen, A. B.; Li, M.; Yang, H.; Batson, P. E.; Greenblatt, M.; Steiner, M. A.; Friedman, D.; Deutsch, T. G.; Garfunkel, E.; Dismukes, G. C., Highly efficient and durable III-V semiconductor-catalyst photocathodes via a transparent protection layer. *Sustainable energy & fuels* **2020**, *4* (3), 1437-1442.
12. Cheng, W.-H.; Richter, M. H.; May, M. M.; Ohlmann, J.; Lackner, D.; Dimroth, F.; Hannappel, T.; Atwater, H. A.; Lewerenz, H.-J., Monolithic photoelectrochemical device for direct water splitting with 19% efficiency. *ACS Energy Letters* **2018**, *3* (8), 1795-1800.
13. Kim, J. H.; Hansora, D.; Sharma, P.; Jang, J.-W.; Lee, J. S., Toward practical solar hydrogen production—an artificial photosynthetic leaf-to-farm challenge. *Chemical Society Reviews* **2019**, *48* (7), 1908-1971.
14. McKone, J. R.; Lewis, N. S.; Gray, H. B., Will solar-driven water-splitting devices see the light of day? *Chemistry of Materials* **2014**, *26* (1), 407-414.
15. Bae, D.; Seger, B.; Vesborg, P. C.; Hansen, O.; Chorkendorff, I., Strategies for stable water splitting via protected photoelectrodes. *Chemical Society Reviews* **2017**, *46* (7), 1933-1954.
16. Khaselev, O.; Turner, J. A., Electrochemical stability of p-GaInP₂ in aqueous electrolytes toward photoelectrochemical water splitting. *Journal of the Electrochemical Society* **1998**, *145* (10), 3335.
17. Gu, H.; Zhang, F.; Hwang, S.; Laursen, A. B.; Liu, X.; Park, S. Y.; Yang, M.; Bramante, R. C.; Hijazi, H.; Kasaei, L.; Feldman, L. C.; Yeh, Y. W.; Batson, P. E.; Larson, B. W.; Li, M.; Li, Y.; Wyatt, K.; Young, J. L.; Teeluck, K.; Zhu, K.; Garfunkel, E.; Dismukes, G. C., Interfacial connections between organic perovskite/n⁺ silicon/catalyst that allow integration of solar cell and catalyst for hydrogen evolution from water. *Advanced Functional Materials* **2023**, 2301196.

18. Song, Z.; Li, C.; Chen, L.; Dolia, K.; Fu, S.; Sun, N.; Li, Y.; Wyatt, K.; Young, J. L.; Deutsch, T. G., All-Perovskite Tandem Photoelectrodes for Unassisted Solar Hydrogen Production. *ACS Energy Letters* **2023**, *8*, 2611-2619.
19. Fehr, A. M.; Agrawal, A.; Mandani, F.; Conrad, C. L.; Jiang, Q.; Park, S. Y.; Alley, O.; Li, B.; Sidhik, S.; Metcalf, I., Integrated halide perovskite photoelectrochemical cells with solar-driven water-splitting efficiency of 20.8%. *Nature Communications* **2023**, *14* (1), 3797.
20. May, M. M.; Lewerenz, H.-J.; Lackner, D.; Dimroth, F.; Hannappel, T., Efficient direct solar-to-hydrogen conversion by in situ interface transformation of a tandem structure. *Nature Communications* **2015**, *6* (1), 1-7.
21. Britto, R. J.; Benck, J. D.; Young, J. L.; Hahn, C.; Deutsch, T. G.; Jaramillo, T. F., Molybdenum disulfide as a protection layer and catalyst for gallium indium phosphide solar water splitting photocathodes. *The journal of physical chemistry letters* **2016**, *7* (11), 2044-2049.
22. Ben-Naim, M.; Britto, R. J.; Aldridge, C. W.; Mow, R.; Steiner, M. A.; Nielander, A. C.; King, L. A.; Friedman, D. J.; Deutsch, T. G.; Young, J. L.; Jaramillo, T. F., Addressing the stability gap in photoelectrochemistry: molybdenum disulfide protective catalysts for tandem III–V unassisted solar water splitting. *ACS Energy Letters* **2020**, *5* (8), 2631-2640.
23. Sun, K.; Liu, R.; Chen, Y.; Verlage, E.; Lewis, N. S.; Xiang, C., A stabilized, intrinsically safe, 10% efficient, solar-driven water-splitting cell incorporating earth-abundant electrocatalysts with steady-state pH gradients and product separation enabled by a bipolar membrane. *Advanced Energy Materials* **2016**, *6* (13), 1600379.
24. Wang, Y.; Schwartz, J.; Gim, J.; Hovden, R.; Mi, Z., Stable unassisted solar water splitting on semiconductor photocathodes protected by multifunctional GaN nanostructures. *ACS Energy Letters* **2019**, *4* (7), 1541-1548.
25. Bansal, A.; Turner, J. A., Suppression of band edge migration at the p-GaN/P2/H2O interface under illumination via catalysis. *The Journal of Physical Chemistry B* **2000**, *104* (28), 6591-6598.
26. Gu, J.; Aguiar, J. A.; Ferrere, S.; Steirer, K. X.; Yan, Y.; Xiao, C.; Young, J. L.; Al-Jassim, M.; Neale, N. R.; Turner, J. A., A graded catalytic–protective layer for an efficient and stable water-splitting photocathode. *Nat Energy* **2017**, *2* (2), 1-8.
27. Moon, C.; Seger, B.; Vesborg, P. C. K.; Hansen, O.; Chorkendorff, I., Wireless photoelectrochemical water splitting using triple-junction solar cell protected by TiO₂. *Cell Reports Physical Science* **2020**, *1* (12).
28. Biunno, N.; Narayan, J.; Hofmeister, S.; Srivatsa, A.; Singh, R., Low-temperature processing of titanium nitride films by laser physical vapor deposition. *Applied physics letters* **1989**, *54* (16), 1519-1521.
29. Chen, Z.; Dinh, H. N.; Miller, E., *Photoelectrochemical water splitting*. Springer: 2013; Vol. 344.
30. Steiner, M. A.; Barraugh, C. D.; Aldridge, C. W.; Alvarez, I. B.; Friedman, D. J.; Ekins-Daukes, N. J.; Deutsch, T. G.; Young, J. L., Photoelectrochemical water splitting using strain-balanced multiple quantum well photovoltaic cells. *Sustainable Energy & Fuels* **2019**, *3* (10), 2837-2844.
31. Hwang, S.; Porter, S. H.; Laursen, A. B.; Yang, H.; Li, M.; Manichev, V.; Calvinho, K. U.; Amarasinghe, V.; Greenblatt, M.; Garfunkel, E.; Dismukes, G. C., Creating stable interfaces between reactive materials: titanium nitride protects photoabsorber–catalyst interface in water-splitting photocathodes. *Journal of Materials Chemistry A* **2019**, *7* (5), 2400-2411.
32. Micic, O.; Sprague, J.; Curtis, C.; Jones, K.; Machol, J.; Nozik, A.; Giessen, H.; Fluegel, B.; Mohs, G.; Peyghambarian, N., Synthesis and characterization of InP, GaP, and GaInP₂ quantum dots. *The Journal of Physical Chemistry* **1995**, *99* (19), 7754-7759.
33. Abdallah, I.; Dupressoire, C.; Laffont, L.; Monceau, D.; Put, A. V., STEM-EELS identification of TiOXNY, TiN, Ti₂N and O, N dissolution in the Ti₂₆4₂S alloy oxidized in synthetic air at 650 C. *Corrosion Science* **2019**, *153*, 191-199.

34. Chourasia, A.; Chopra, D., X-ray photoelectron study of TiN/SiO₂ and TiN/Si interfaces. *Thin Solid Films* **1995**, *266* (2), 298-301.
35. Green, M. A., Solar cell fill factors: General graph and empirical expressions. *Solid State Electronics* **1981**, *24* (8), 788-789.
36. Varadhan, P.; Fu, H.-C.; Kao, Y.-C.; Horng, R.-H.; He, J.-H., An efficient and stable photoelectrochemical system with 9% solar-to-hydrogen conversion efficiency via InGaP/GaAs double junction. *Nature Communications* **2019**, *10* (1), 5282.